Partially coherent surface plasmon polaritons

2016 EPL 116 64001

(http://iopscience.iop.org/0295-5075/116/6/64001)

A Letters Journal Exploring the Frontiers of Physics

December 2016

EPL, **116** (2016) 64001 www.epljournal.org
doi: 10.1209/0295-5075/116/64001

Partially coherent surface plasmon polaritons

Andreas Norrman[1], Sergey A. Ponomarenko[2] and Ari T. Friberg[1]

[1] *Institute of Photonics, University of Eastern Finland - P.O. Box 111, FI-80101 Joensuu, Finland*
[2] *Department of Electrical and Computer Engineering, Dalhousie University - Halifax, Nova Scotia, B3J 2X4, Canada*

received 14 November 2016; accepted in final form 9 January 2017
published online 3 February 2017

PACS 42.25.-p – Wave optics
PACS 42.25.Kb – Coherence
PACS 73.20.Mf – Collective excitations (including excitons, polarons, plasmons and other charge-density excitations)

Abstract – We formulate a framework to tailor the electromagnetic coherence of polychromatic surface plasmon polaritons (SPPs) at a metal-air interface by controlling the correlations of the excitation light. The formalism covers stationary and nonstationary SPP fields of arbitrary spectra. We show that narrowband SPPs are virtually propagation invariant and strictly polarized, whereas the coherence properties of broadband SPPs can be widely tuned to specific applications. The connection between the coherence state of the light source and the ensuing SPP field establishes a novel paradigm in statistical plasmonics with far-reaching implications for plasmon coherence engineering.

Introduction. – Surface waves are ubiquitous in physics; they arise in fields as diverse as fluid mechanics, acoustics, geophysics, and electromagnetics. Surface electromagnetic waves especially have attracted interest in science and engineering [1]. Among them are the celebrated surface polaritons, supported as plasmons, phonons, and excitons. Surface plasmon polaritons (SPPs) [2] have been the workhorse in nanophotonics [3], resulting in the emergence of plasmonics as a separate field covering cross-disciplinary physics, including holography [4], novel materials [5,6], nonlinear interactions [7,8], and subwavelength light control [9]. To date, plasmonics has chiefly dealt with spatially and spectrally fully coherent SPPs. Coherence, however, is an indispensable degree of freedom governing spectral distribution, propagation, interference, polarization, and interactions of classical and quantum wave fields of diverse nature [10]. Thus, besides their unique role in shaping the salient features of surface electromagnetic waves, SPP coherence properties are of fundamental interest for wave and surface physics in general.

Surface plasmons are known to greatly alter the spectrum, polarization, and spatial coherence of optical near fields [11–14]. Polar material with grating etched on the surface produces, in thermal equilibrium, spatially coherent beam lobes of directionally dependent spectrum [15]. SPPs also play a key role in modifying the coherence properties of fields transmitted through periodic hole arrays in metal films [16,17]. In particular, it has been demonstrated both theoretically [18] and experimentally [19] that SPPs may be employed to control the spatial coherence between optical fields in Young's two-slit interferometer. And conversely, Young's setup combined with leakage radiation microscopy enables the measurement of SPP coherence evolution on propagation [20]. Further, bi-modal fields composed of uncorrelated long-range and short-range SPPs on a metallic nanoslab were studied and their coherence properties elucidated [21]. However, to our knowledge, no systematic theory of multimode, spatially and spectrally partially coherent SPPs has so far been developed. Exploring the statistical features and excitation mechanisms of polychromatic SPP fields in space-time domain presents a fundamental interest. By the same token, coherence-tailored polychromatic SPPs are expected to serve as versatile tools, *e.g.*, for plasmon continuum spectroscopy [22], on-chip ultrashort optical pulse manipulation in nanostructured optoelectronic circuits [23], controlled coupling of light-emitting elements [24–26], and subwavelength white-light imaging [27].

In this work, we advance a theory for partially coherent polychromatic SPP fields of arbitrary spectra generated at a metal-air boundary. In particular, we determine the space-time and space-frequency coherence matrices of multicomponent SPP fields in terms of the spectral correlations of their monochromatic constituents. As a key

result, we demonstrate how such polychromatic SPP fields can be excited with partially coherent beam sources in the Kretschmann coupling modality. We establish that the SPP coherence characteristics can be widely tailored by controlling the spectral and spatial coherence of the light source. We show that narrowband SPPs are fully polarized and virtually propagation invariant over distances comparable to the propagation lengths determined by the losses in the metal. Such propagation-invariant SPPs will facilitate nearly distortion-free information transfer in plasmonic networks. We also present spectrally broadband SPPs of widely variable coherence, retaining a high degree of polarization. Our work represents a novel paradigm in statistical plasmonics, referred to as plasmon coherence engineering, which we expect to be instrumental, among others, for sensor applications, interferometry, spectroscopy, surface morphology studies, and nanoparticle excitation.

Formalism. – We begin by recalling the excitation of a single SPP mode of (angular) frequency ω in the Kretschmann configuration [2,3], sketched in fig. 1, with a homogeneous, isotropic, and nonmagnetic metal film deposited on a glass prism. The film, located in the xy-plane and of complex-valued relative permittivity $\epsilon_{\rm r}(\omega)$, is taken to be thick enough so that any coupling between the metal-slab modes [28,29] can be neglected. The region near the metal-air surface at $z = 0$ can then be treated as semi-infinite half-spaces [30] and the x-axis is chosen to coincide with the SPP propagation direction. As only TM-polarized SPPs are supported by nonmagnetic media [2,3], the polychromatic electric field in air, at a space-time point $(\mathbf{r}, t)$, can be written as [30]

$$\mathbf{E}(\mathbf{r},t) = \int_{\omega_-}^{\omega_+} E(\omega)\hat{\mathbf{p}}(\omega)\mathrm{e}^{\mathrm{i}[\mathbf{k}(\omega)\cdot\mathbf{r}-\omega t]}\mathrm{d}\omega, \tag{1}$$

where $\omega_{+,-}$ specify the SPP frequency domain (in the undamped free-electron model which ignores absorption $\omega_+ = \omega_{\rm p}/\sqrt{2}$, with $\omega_{\rm p}$ being the plasma frequency [2]). Further, $E(\omega)$ is a complex spectral amplitude of the monochromatic SPP at the origin ($\mathbf{r} = 0$) and

$$\mathbf{k}(\omega) = k_x(\omega)\hat{\mathbf{e}}_x + k_z(\omega)\hat{\mathbf{e}}_z, \tag{2}$$

$$\hat{\mathbf{p}}(\omega) = \hat{\mathbf{k}}(\omega) \times \hat{\mathbf{e}}_y \tag{3}$$

are the wave vector and the normalized polarization vector, respectively, with $\hat{\mathbf{k}}(\omega) = \mathbf{k}(\omega)/|\mathbf{k}(\omega)|$, and $\hat{\mathbf{e}}_x$, $\hat{\mathbf{e}}_y$, and $\hat{\mathbf{e}}_z$ are Cartesian unit vectors. We note that $\hat{\mathbf{p}}(\omega)$ is not orthogonal to $\mathbf{k}(\omega)$ [29], implying that the SPP mode is elliptically polarized (in the xz-plane). It follows from the electromagnetic boundary conditions that [2,3,30]

$$k_x(\omega) = \frac{\omega}{c}\sqrt{\frac{\epsilon_{\rm r}(\omega)}{\epsilon_{\rm r}(\omega)+1}}, \quad k_z(\omega) = \frac{\omega}{c}\sqrt{\frac{1}{\epsilon_{\rm r}(\omega)+1}}, \tag{4}$$

where c is the speed of light. The propagation length of a monochromatic SPP component is given by

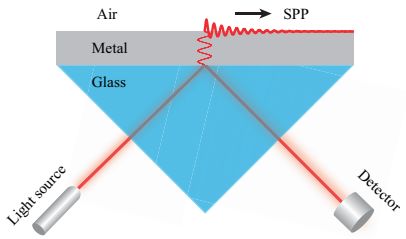

Fig. 1: (Colour online) SPP excitation in the Kretschmann configuration.

$l_{\rm SPP}(\omega) = 1/k_x''(\omega)$, with the double prime denoting the imaginary part.

The complete information about the second-order statistical properties of a nonstationary and generally three-component electric field, at two space-time points $(\mathbf{r}_1, t_1)$ and $(\mathbf{r}_2, t_2)$, is encoded in the electric coherence matrix

$$\mathbf{\Gamma}(\mathbf{r}_1,t_1;\mathbf{r}_2,t_2) = \langle \mathbf{E}^*(\mathbf{r}_1,t_1)\mathbf{E}^{\rm T}(\mathbf{r}_2,t_2)\rangle. \tag{5}$$

Here $\mathbf{E}(\mathbf{r}, t)$ is a column vector, the asterisk and superscript "T" denote complex conjugation and matrix transpose, respectively, and the angle brackets stand for ensemble averaging. Now, let eq. (1) be a realization of the random electric field. All coherence (and polarization) properties of the polychromatic SPP field are then obtained by inserting eq. (1) into eq. (5), yielding

$$\mathbf{\Gamma}(\mathbf{r}_1,t_1;\mathbf{r}_2,t_2) = \int_{\omega_-}^{\omega_+}\int_{\omega_-}^{\omega_+} \mathbf{W}(\mathbf{r}_1,\omega_1;\mathbf{r}_2,\omega_2), \times \mathrm{e}^{-\mathrm{i}(\omega_2 t_2-\omega_1 t_1)}\mathrm{d}\omega_1\mathrm{d}\omega_2, \tag{6}$$

in which

$$\mathbf{W}(\mathbf{r}_1,\omega_1;\mathbf{r}_2,\omega_2) = W(\omega_1,\omega_2)\mathbf{K}(\omega_1,\omega_2) \times \mathrm{e}^{\mathrm{i}[\mathbf{k}(\omega_2)\cdot\mathbf{r}_2-\mathbf{k}^*(\omega_1)\cdot\mathbf{r}_1]} \tag{7}$$

is the spectral electric coherence matrix, with

$$W(\omega_1,\omega_2) = \langle E^*(\omega_1)E(\omega_2)\rangle \tag{8}$$

being the spectral correlation function and

$$\mathbf{K}(\omega_1,\omega_2) = [|\mathbf{k}(\omega_1)||\mathbf{k}(\omega_2)|]^{-1} \times \begin{bmatrix} k_z^*(\omega_1)k_z(\omega_2) & -k_z^*(\omega_1)k_x(\omega_2) \\ -k_x^*(\omega_1)k_z(\omega_2) & k_x^*(\omega_1)k_x(\omega_2) \end{bmatrix}. \tag{9}$$

Equation (6) is general in the sense that no restrictions have been imposed on the relative permittivity, the spectrum, or the spectral correlation function; it covers any partially coherent polychromatic SPP field. In particular, the function $W(\omega_1, \omega_2)$ in eq. (8) specifies fully the space-frequency, and thus also the space-time, coherence characteristics of the SPP field.

Plasmon coherence engineering. – The crux of plasmon coherence engineering is to judiciously tailor $W(\omega_1, \omega_2)$ by light sources of controlled coherence, as we demonstrate next. To this end, we first examine a TM-polarized, partially coherent, polychromatic beam incident on the prism in the geometry of fig. 1. The electric field of the incoming light can be expressed by the angular spectrum representation [3,10] as

$$\mathcal{E}(\mathbf{r}, t) = \int_0^\infty \Big[\int_{-\infty}^{\infty} \mathcal{E}(k_X, \omega) \hat{\mathbf{p}}(k_X, \omega) \times \mathrm{e}^{\mathrm{i}(k_X X + k_Z Z)} \mathrm{d}k_X \Big] \mathrm{e}^{-\mathrm{i}\omega t} \mathrm{d}\omega, \quad (10)$$

where $k_X^2 + k_Z^2 = n^2(\omega/c)^2$, with n being the refractive index of the prism. A coordinate frame XZ, with the Z-axis making an angle θ_0 with respect to the z-axis of the xz-frame, has been introduced. The second-order statistical properties of the incident field are then specified by the spectral electric correlation function

$$\mathcal{W}(k_{1X}, \omega_1; k_{2X}, \omega_2) = \langle \mathcal{E}^*(k_{1X}, \omega_1) \mathcal{E}(k_{2X}, \omega_2) \rangle. \quad (11)$$

We further choose θ_0 such that in the xz-frame the tangential wave vector component of the beam mode of central frequency ω_0 and $k_X = 0$ within the angular spectrum exactly corresponds to $k'_x(\omega_0)$ of the SPP obtained from eq. (4), with the prime denoting the real part, *i.e.*,

$$n \frac{\omega_0}{c} \sin\theta_0 = k'_x(\omega_0). \quad (12)$$

This condition represents precise phase matching between the central illuminating plane wave and the central SPP mode along the metal-air surface.

To ensure that an SPP mode is generated at every ω within the spectral excitation bandwidth, one must impose a similar phase matching condition for the other illumination plane waves as well. Suppose that for an arbitrary frequency $\omega \neq \omega_0$ the angular spectrum mode with $k_X = n(\omega/c)\sin\Delta\theta$, where $\Delta\theta$ is the angle between the wave vector and the Z-axis, couples to the corresponding SPP. In the xz-frame this means that

$$n \frac{\omega}{c} \sin\theta = k_Z \sin\theta_0 + k_X \cos\theta_0 = k'_x(\omega), \quad (13)$$

with $\theta = \theta_0 + \Delta\theta$, and by making use of the paraxiality of the illumination so that $\Delta\theta \approx k_X/k_Z \ll \theta_0$ and $k_Z \approx n(\omega/c)$, from eqs. (12) and (13) we obtain the coupling condition

$$k_X = \frac{k'_x(\omega) - k'_x(\omega_0)}{\cos\theta_0}. \quad (14)$$

At each frequency ω within the bandwidth the angular spectrum wave satisfying eq. (14) thus excites the respective monochromatic SPP constituent. Now, since the spectral amplitudes in eqs. (1) and (10) are connected as $E(\omega) \propto \mathcal{E}(k_X, \omega)$, with the exact coupling efficiency specified by the transmission coefficient of the metal slab (see appendix), we find from eq. (14) that

$$E(\omega) \propto \mathcal{E}\Big[\frac{k'_x(\omega) - k'_x(\omega_0)}{\cos\theta_0}, \omega\Big]. \quad (15)$$

The relation between the SPP correlation function in eq. (8) and the angular spectrum correlation function of the incident light given by eq. (11) thus reads as

$$W(\omega_1, \omega_2) \propto \mathcal{W}\Big[\frac{k'_x(\omega_1) - k'_x(\omega_0)}{\cos\theta_0}, \omega_1; \frac{k'_x(\omega_2) - k'_x(\omega_0)}{\cos\theta_0}, \omega_2\Big]. \quad (16)$$

Knowing the dispersion of the metal, eq. (16) establishes exactly how the spatio-spectral statistical properties of the stationary or pulsed excitation beam are to be tuned to create a polychromatic SPP field with the desired coherence characteristics.

The scheme for controlled generation of spatially and spectrally (temporally) partially coherent, polychromatic SPPs at the metal-air interface is the cornerstone in plasmon coherence engineering. The achievable SPP bandwidth can be estimated from the (paraxial) coupling condition in eq. (14) by knowing $k'_x(\omega)$ and θ_0 for a given metal. For example, assuming $\Delta\theta < 5^\circ$ and $n \approx 1.5$, and employing empirical data [31] leads for central wavelength $\lambda_0 = 650\,\mathrm{nm}$ in the case of Ag to $\theta_0 \approx 43.4^\circ$ and $595\,\mathrm{nm} < \lambda < 706\,\mathrm{nm}$. The illuminating light source then must possess (at least) the same spectral bandwidth, with desired correlations among the different frequencies as specified by eq. (16). As a last step, the frequency components are to be directed as plane waves at the correct angles given by eq. (14), which can be accomplished by spectrally separating the frequencies from a polychromatic plane-wave source, or by employing spatially partially coherent light beams [10]. Although the scheme for plasmon coherence engineering presented here concerns one-dimensional SPP propagation, with appropriate modifications the same ideas naturally apply for statistical plasmonics in two dimensions, as in tailoring the electromagnetic coherence of optical evanescent fields at a dielectric interface [32].

Examples. – To gain insight into the coherence characteristics of polychromatic SPPs, we first consider a narrowband field of central frequency ω_0. Under the condition that metal dispersion can be ignored, *i.e.*, $\epsilon_\mathrm{r}(\omega) \approx \epsilon_\mathrm{r}(\omega_0)$, we may extend all frequency integrations from minus infinity to plus infinity. It then follows from eqs. (2) and (4) that $\mathbf{k}(\omega) \approx (\omega/c)\boldsymbol{\kappa}(\omega_0)$, with $\boldsymbol{\kappa}(\omega_0) = (c/\omega_0)\mathbf{k}(\omega_0)$, and further from eqs. (6)–(9) that

$$\boldsymbol{\Gamma}(\mathbf{r}_1, t_1; \mathbf{r}_2, t_2) = \mathbf{K}(\omega_0, \omega_0) \int_{-\infty}^{\infty}\int_{-\infty}^{\infty} W(\omega_1, \omega_2) \times \mathrm{e}^{\mathrm{i}[\alpha_2(\mathbf{r}_2, t_2) - \alpha_1^*(\mathbf{r}_1, t_1)]} \mathrm{d}\omega_1 \mathrm{d}\omega_2, \quad (17)$$

where

$$\alpha_j(\mathbf{r}_j, t_j) = \frac{\omega_j}{c}[\boldsymbol{\kappa}(\omega_0) \cdot \mathbf{r}_j - c t_j], \quad (18)$$

with $j \in \{1,2\}$. Equation (17) implies that all the coherence matrix elements have identical space-time dependence, *i.e.*, the correlations among the field components propagate and attenuate in exactly the same way. Moreover, if we let $x_1 = x_2 = x$, and recall that for a sufficiently narrowband spectrum the SPP modes decay roughly at the same rate, we find from eq. (17) that $\mathbf{\Gamma}(\mathbf{r}_1, t_1; \mathbf{r}_2, t_2) \propto \exp[-2x/l_{\mathrm{SPP}}(\omega_0)]$. Hence, over distances smaller than $l_{\mathrm{SPP}}(\omega_0)$ the polychromatic narrowband SPP fields are virtually propagation invariant. Such SPPs can be used for nearly distortion-free information or image transfer in plasmonic networks.

For broadband spectra, on the other hand, dispersion in the metal can no longer be neglected and thus each element of the coherence matrix in eq. (6) has to be treated separately (and numerically), whereupon the correlations between the electric-field components will in general have different space-time evolutions. It is therefore convenient to analyze the ensuing SPPs in terms of the electromagnetic degree of coherence [33],

$$\gamma(\mathbf{r}_1, t_1; \mathbf{r}_2, t_2) = \frac{||\mathbf{\Gamma}(\mathbf{r}_1, t_1; \mathbf{r}_2, t_2)||_{\mathrm{F}}}{\sqrt{\mathrm{tr}\mathbf{J}(\mathbf{r}_1, t_1)\mathrm{tr}\mathbf{J}(\mathbf{r}_2, t_2)}}, \qquad (19)$$

where $\|\cdot\|_{\mathrm{F}}$ is the Frobenius norm, tr denotes the trace, and $\mathbf{J}(\mathbf{r}_j, t_j) = \mathbf{\Gamma}(\mathbf{r}_j, t_j; \mathbf{r}_j, t_j)$ is the polarization matrix. The degree of coherence in eq. (19), which is real and bounded as $0 \leq \gamma(\mathbf{r}_1, t_1; \mathbf{r}_2, t_2) \leq 1$, is a measure of all the correlations existing in a multicomponent light field. The upper and lower limits correspond to full coherence and complete lack of coherence of the electric vector field at the two space-time points, while the intermediate values represent partial coherence.

The spectra of broadband SPP fields are determined by the spectral correlation functions $W(\omega_1, \omega_2)$ which, as shown above, are sculpted into the desired form by modifying the spectral (and spatial) coherence of the excitation light. As an example, we examine spectrally uncorrelated (stationary) SPPs, in which case $\mathbf{\Gamma}(\mathbf{r}_1, t_1; \mathbf{r}_2, t_2) = \mathbf{\Gamma}(\mathbf{r}_1, \mathbf{r}_2, \tau)$ with $\tau = t_2 - t_1$. Stationary illumination is expected to give a lower boundary for SPP coherence, since any spectral correlations would lead to a more coherent field. It is useful to focus on the longitudinal coherence at the surface ($z_1 = z_2 = 0$), where the field is strongest. We let $x_1 = 0$ mark the SPP excitation point and denote $x_2 = x$. Figure 2 illustrates the equal-time ($\tau = 0$) degree of longitudinal coherence $\gamma(x)$ at an Ag-air interface for SPP fields with Gaussian (wavelength) spectra of different widths. The coherence length, which naturally decreases as the spectral width is increased, is seen to extend over several wavelengths while still only a fraction of the SPP propagation distance. For ultrawide spectra, such as thermal radiation, the coherence length is on the order of the mean wavelength. Allowing nonzero correlations in $W(\omega_1, \omega_2)$, as in the Gaussian Schell-model [10], renders the SPP field more coherent and nonstationary. At high levels of spectral correlations the SPPs become pulses that propagate at the metal surface.

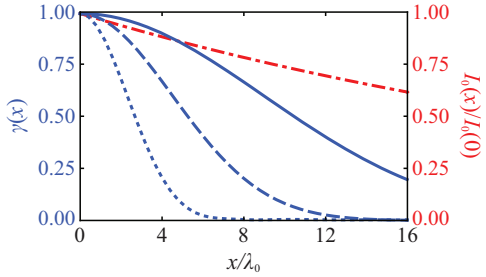

Fig. 2: (Colour online) Equal-time degree of longitudinal coherence $\gamma(x)$ for a Gaussian SPP field of central SPP wavelength $\lambda_0 = 632.8\,\mathrm{nm}$ at an Ag-air interface, when the spectral width (standard deviation $\Delta\lambda$ in wavelength) is varied: $\Delta\lambda = 10\,\mathrm{nm}$ (solid blue curve), $\Delta\lambda = 20\,\mathrm{nm}$ (dashed blue curve), and $\Delta\lambda = 40\,\mathrm{nm}$ (dotted blue curve). The dash-dotted red curve depicts the normalized SPP intensity $I_0(x)/I_0(0)$ for λ_0. The relative permittivity of Ag is obtained from the empirical data of [31].

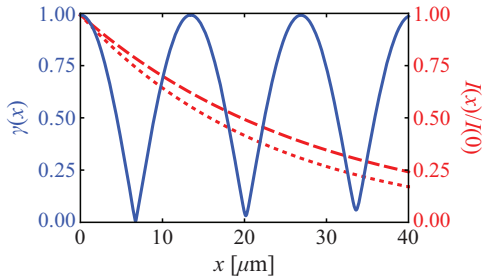

Fig. 3: (Colour online) Equal-time degree of longitudinal coherence $\gamma(x)$ (solid blue curve) for an SPP field excited by two independent Kr lasers of wavelengths $\lambda_1 = 676.4\,\mathrm{nm}$ and $\lambda_2 = 647.1\,\mathrm{nm}$ at an Ag-air interface. The dashed and dotted curves show the normalized intensities $I(x)/I(0)$ for the spectral SPP components of λ_1 and λ_2, respectively. The relative permittivity of Ag is obtained from the empirical data of [31].

As an illustration of strong SPP coherence modulation, we consider an SPP field composed of two mutually uncorrelated spectral components. If the intensities of the two constituents are equal at the excitation point $\mathbf{r}_1 = 0$, eqs. (6)–(9) and (19) yield for the degree of coherence

$$\gamma(\mathbf{r}, \tau) = \frac{1}{\sqrt{2}}\sqrt{1 + p\frac{\cos(\Delta\mathbf{k}' \cdot \mathbf{r} - \Delta\omega\tau)}{\cosh(\Delta\mathbf{k}'' \cdot \mathbf{r})}}, \qquad (20)$$

where $\mathbf{r} = \mathbf{r}_2$, $\Delta\omega = \omega_2 - \omega_1$, $\Delta\mathbf{k}' = \mathbf{k}'(\omega_2) - \mathbf{k}'(\omega_1)$, $\Delta\mathbf{k}'' = \mathbf{k}''(\omega_2) - \mathbf{k}''(\omega_1)$, and $p = |\hat{\mathbf{p}}^*(\omega_1) \cdot \hat{\mathbf{p}}(\omega_2)|^2$. The degree of coherence in eq. (20) is illustrated in fig. 3 for $z = \tau = 0$, *i.e.*, $\gamma(\mathbf{r}, \tau) = \gamma(x)$, when the SPP constituents are generated by two independent Kr lasers at an Ag-air interface. We emphasize that the oscillation of $\gamma(x)$, caused by the cosine term, does not result from conventional wave beating, since the two SPP constituents are uncorrelated and hence do not interfere. Instead, the oscillation originates from the fact that at certain periodic distances the electromagnetic SPP field is statistically similar [34,35] to the total field at the excitation

point. At the locations where $\gamma(x)$ is high, or low, the SPP would interact with nanoparticles in the vicinity of the surface in a coherent, or incoherent, manner. This could be used, for instance, for controlled excitation of random sets of molecules or quantum dots [25].

Polarization. – Regarding polarization, the electric field in eq. (1) has two components that lie in the same (xz) plane as the wave vectors of the single-mode SPPs. Although this situation differs physically from an ordinary light beam, for which the electric field is perpendicular to the propagation direction, for the analysis of the SPP polarization state we may nonetheless employ the conventional formalism of two-component beam fields [21]. Hence, in our case, the degree of polarization of the polychromatic SPP field is defined through [10]

$$P(\mathbf{r},t)=\sqrt{2\frac{\mathrm{tr}\mathbf{J}^2(\mathbf{r},t)}{\mathrm{tr}^2\mathbf{J}(\mathbf{r},t)}-1}, \tag{21}$$

satisfying $0 \leq P(\mathbf{r},t) \leq 1$. In this way eq. (21) characterizes the polarization state of the SPP electric field in the plane of plasmon propagation at a single space-time point. For the narrowband case it readily follows from eqs. (17) and (21) that $P(\mathbf{r},t)=1$, indicating that narrowband SPP fields are completely polarized everywhere, regardless of the spectral correlations. This result is supported by the physical fact that a monochromatic SPP is fully (elliptically) polarized.

Quite surprisingly, also the broadband SPP fields remain highly polarized. This finding, which might appear counterintuitive, can be understood as follows. Suppose that, at a given reference point, the polychromatic SPP field has a broad bandwidth with the individual spectral modes being uncorrelated and roughly of equal intensity. These choices are expected to give the fundamental lower limit for the polarization degree of the broadband SPP field, since any spectral correlations or spectral density variations would lead to a more polarized field. But, even though the equal-intensity SPP constituents are spectrally fully uncorrelated, their polarization vectors in eq. (3) are very similar, at least within the optical regime, rendering the polychromatic SPP field strongly polarized. On propagation away from the reference point the spectrum narrows down, since the modes pertaining to the high-frequency end of the spectrum decay faster than those in the lower spectral range [22], making the SPP field even more polarized.

Conclusions. – In summary, by utilizing rigorous electromagnetic coherence theory, we have formulated a framework for polychromatic, partially coherent, multicomponent SPP fields excited at a metal-air interface. The general space-time coherence matrix, valid for both stationary and nonstationary SPP fields of arbitrary spectra and spectral correlations, was analytically derived. It was particularly demonstrated how spectrally partially correlated SPPs can be excited with partially coherent beams

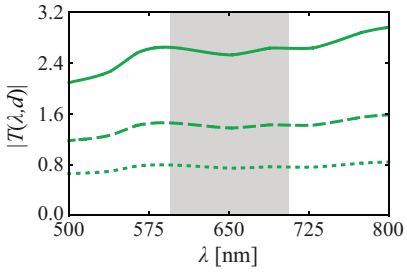

Fig. 4: (Colour online) Magnitude of the slab transmission coefficient $T(\lambda,d)$ under the phase matching condition of eq. (13) for an Ag film as a function of the wavelength λ, when the slab thickness is varied: $d=100\,\mathrm{nm}$ (solid green curve), $d=115\,\mathrm{nm}$ (dashed green curve), and $d=130\,\mathrm{nm}$ (dotted green curve). The shaded region represents the SPP bandwidth $595\,\mathrm{nm}<\lambda<706\,\mathrm{nm}$, achieved by paraxial illumination with a spread angle $\Delta\theta=5^\circ$ (see discussion below eq. (16)). The refractive index of the glass prism is taken to be $n=1.5$, whereas the relative permittivity of Ag is obtained from the empirical data of [31].

in the customary Kretschmann configuration. This is the key result of plasmon coherence engineering: with knowledge of the metal's dispersion our method allows exact determination of the spatio-spectral coherence of the exciting light to generate polychromatic SPPs with desired coherence properties. We further showed that in the narrowband limit the SPP field is virtually propagation invariant and strictly polarized and that even broadband SPPs, while widely coherence tunable, remain strongly polarized. The polychromatic SPP fields of controlled coherence thus provide versatile tools for various future surface-photonic applications.

* * *

This research was supported by the National Science and Engineering Research Council of Canada and by the Academy of Finland (project 268480). AN especially acknowledges the Jenny and Antti Wihuri Foundation and the Emil Aaltonen Foundation.

Appendix: coupling efficiency. – The coupling between the angular spectrum mode of the illumination, $\mathcal{E}(k_X,\omega)$, with k_X satisfying eq. (14), and the ensuing SPP spectral component, $E(\omega)$, is given by the transmission coefficient of the slab [36]

$$T(\omega,d)=\frac{t_{12}(\omega)t_{23}(\omega)\mathrm{e}^{\mathrm{i}k_{z2}(\omega)d}}{1+r_{12}(\omega)r_{23}(\omega)\mathrm{e}^{2\mathrm{i}k_{z2}(\omega)d}}. \tag{A.1}$$

Here $t_{12}(\omega)$ and $r_{12}(\omega)$ ($t_{23}(\omega)$ and $r_{23}(\omega)$) are, respectively, the Fresnel transmission and reflection coefficients for the glass-metal (metal-air) interface, $k_{z2}(\omega)$ is the normal wave vector component in the metal, and d is the thickness of the slab. Any variation in $T(\omega,d)$ may, however, be compensated by changing $\mathcal{E}(k_X,\omega)$, since only their product matters in plasmon engineering.

As an illustration, fig. 4 shows the behavior of $|T(\lambda, d)|$ as a function of the wavelength λ for Ag slabs of different thicknesses. It is seen that $|T(\lambda, d)|$ varies relatively smoothly over a broad spectral range. In particular, within the 100 nm bandwidth centered at $\lambda = 650\,\mathrm{nm}$ (shaded area in fig. 4), corresponding to illumination with a paraxial polychromatic beam of angular spread $\Delta\theta = 5°$, discussed below eq. (16), the coupling efficiency is spectrally quite flat regardless of d. As the slab thickness increases, the coupling strength decreases, due to absorption, and becomes practically independent of the wavelength.

REFERENCES

[1] Polo J. A. jr., Mackay T. G. and Lakhtakia A., *Electromagnetic Surface Waves* (Elsevier, Amsterdam) 2013.

[2] Maier S. A., *Plasmonics: Fundamentals and Applications* (Springer, Berlin) 2007.

[3] Novotny L. and Hecht B., *Principles of Nano-Optics*, 2nd edition (Cambridge University Press, Cambridge) 2012.

[4] Ozaki M., Kato J.-I. and Kawata S., *Science*, **332** (2011) 218.

[5] Boltasseva A. and Atwater H. A., *Science*, **331** (2011) 290.

[6] Grigorenko A. N., Polini M. and Novoselov K. S., *Nat. Photon.*, **6** (2012) 749.

[7] Kauranen M. and Zayats A. V., *Nat. Photon.*, **6** (2012) 737.

[8] Wang L., Che F., Ponomarenko S. A. and Chen Z. D., *Opt. Express*, **21** (2013) 14159.

[9] Gramotnev D. K. and Bozhevolnyi S. I., *Nat. Photon.*, **4** (2010) 83.

[10] Mandel L. and Wolf E., *Optical Coherence and Quantum Optics* (Cambridge University Press, Cambridge) 1995.

[11] Carminati R. and Greffet J.-J., *Phys. Rev. Lett.*, **82** (1999) 1660.

[12] Shchegrov A. V., Joulain K., Carminati R. and Greffet J.-J., *Phys. Rev. Lett.*, **85** (2000) 1548.

[13] Setälä T., Kaivola M. and Friberg A. T., *Phys. Rev. Lett.*, **88** (2002) 123902.

[14] Ellis J., Dogariu A., Ponomarenko S. and Wolf E., *Opt. Commun.*, **248** (2005) 333.

[15] Greffet J.-J., Carminati R., Joulain K., Mulet J.-P., Mainguy S. and Chen Y., *Nature*, **416** (2002) 61.

[16] Gan C. H., Gu Y., Visser T. D. and Gbur G., *Plasmonics*, **7** (2012) 313.

[17] Saastamoinen T. and Lajunen H., *Opt. Lett.*, **38** (2013) 5000.

[18] Gan C. H., Gbur G. and Visser T. D., *Phys. Rev. Lett.*, **98** (2007) 043908.

[19] Divitt S., Frimmer M., Visser T. D. and Novotny L., *Opt. Lett.*, **41** (2016) 3094.

[20] Aberra Guebrou S., Laverdant J., Symonds C., Vignoli S. and Bellessa J., *Opt. Lett.*, **37** (2012) 2139.

[21] Norrman A., Setälä T. and Friberg A. T., *Opt. Express*, **23** (2015) 20696.

[22] Bouhelier A. and Wiederrecht G. P., *Phys. Rev. B*, **71** (2005) 195406.

[23] Ozbay E., *Science*, **311** (2006) 189.

[24] Koller D. M., Hohenau A., Ditlbacher H., Galler N., Reil F., Aussenegg F. R., Leitner A., List E. J. W. and Krenn J. R., *Nat. Photon.*, **2** (2008) 684.

[25] Aberra Guebrou S., Symonds C., Homeyer E., Plenet J. C., Gartstein Yu. N., Agranovich V. M. and Bellessa J., *Phys. Rev. Lett.*, **108** (2012) 066401.

[26] Shi L., Hakala T. K., Rekola H. T., Martikainen J.-P., Moerland R. J. and Törmä P., *Phys. Rev. Lett.*, **112** (2014) 153002.

[27] Liu W., Neshev D. N., Miroshnichenko A. E., Shadrivov I. V. and Kivshar Y. S., *Phys. Rev. B*, **83** (2011) 073404.

[28] Norrman A., Setälä T. and Friberg A. T., *Opt. Express*, **22** (2014) 4628.

[29] Norrman A., Setälä T. and Friberg A. T., *Phys. Rev. A*, **90** (2014) 053849.

[30] Norrman A., Setälä T. and Friberg A. T., *Opt. Lett.*, **38** (2013) 1119.

[31] Palik E. D. (Editor), *Handbook of Optical Constants of Solids* (Academic Press, Orlando) 1998.

[32] Norrman A., Setälä T. and Friberg A. T., *Opt. Lett.*, **40** (2015) 5216.

[33] Tervo J., Setälä T. and Friberg A. T., *Opt. Express*, **11** (2003) 1137.

[34] Ponomarenko S. A., Roychowdhury H. and Wolf E., *Phys. Lett. A*, **345** (2005) 10.

[35] Voipio T., Setälä T. and Friberg A. T., *J. Opt. Soc. Am. A*, **32** (2015) 741.

[36] Maradudin A. A., Sambles J. R. and Barnes W. L., *Modern Plasmonics* (Elsevier, Amsterdam) 2014.